RSC Advances

PAPER

View Article Online
View Journal | View Issue

Published on 20 July 2016. Downloaded by Southeast University - Jiulonghu Campus on 25/12/2016 13:59:32.

Cite this: *RSC Adv.*, 2016, **6**, 68964

Multiple value storage based on a nano-electronic–mechanical mechanism using graphene flakes†

Neng Wan,*[a] Wei Pan[b] and Shao-chun Tang[c]

Received 29th April 2016
Accepted 7th July 2016

DOI: 10.1039/c6ra11115g

www.rsc.org/advances

We report here a nano-electronic–mechanical storage mechanism with graphene flakes (GFs) revealed by *in situ* transmission electron microscopy observations accompanied by nano-manipulation and probing of electrical properties. Repeatable two- and three- level state storage was demonstrated using two GFs nanoelectrodes with evident hysteresis properties. The detailed mechanisms, including the formation and rupture of the GFs contact as well as the corresponding electrical properties of the hysteresis, were visualized directly. Due to the high mechanical stability and outstanding electrical conductivity of the graphene, the hysteresis property is quite stable, which allows multi-value storage in this system. This work provides a route to achieve multiple value storage based on the nano-electronic–mechanical storage mechanism.

Introduction

Data storage is one of the most important aspects of modern electrical devices. Current data storage techniques are realized based on various mechanisms, such as rewritable compact disks, which use signals obtained by optical reflection from phase change materials, flash memory, which involves charge storage in dielectric materials, and hard disks, which exploit the giant magnetoresistance effect.[1,2] It is widely accepted that techniques used for data storage should show hysteresis properties. This supplies a storage window wherein the data can be stored in the corresponding state. The demand for higher storage density has continued during the past decades. One route to achieve high storage density is to diminish the size of the data storage unit until a technical or physical limit is encountered. Another route is to use multiple value storage instead of binary value storage.[3] Binary storage uses "low" and "high" current/voltage levels as "0" and "1" signals in modern digital circuits, while multiple value storage may use more states. For example, three-level type storage has "0", "1", and "2" signals; thus, it provides three states. Multiple values increase the storage density rapidly according to S^n, with "S" being the usable state and "n" being the number of storage units. Theoretically, 100 storage units will result in storage capacity that is enlarged $\sim 10^{17}$ times ($= 1.5^{100}$) simply by replacing, for example, two-level storage with three-level storage. Thus, achieve multiple value storage is highly desirable.

There have been many studies on multiple value storage. Different material systems and device structures have been demonstrated. Examples include semiconductor materials with an $Au/BiFe_{0.95}Mn_{0.05}O_3/La_{5/8}Ca_{3/8}MnO_3$ heterostructure,[4] dielectrical materials of lead zirconate titanate,[5] insulator materials of silicon monoxide,[6] and hybrid materials of graphene–ferroelectric composites.[3] Some new device structures were also suggested based on graphene structures.[7,8] Recent studies normally use the current–voltage relationship to illustrate the existence of multiple value storage mechanisms, and the physical origin is of great interest. However, due to the complex conduction mechanisms of the different materials, as well as their strong relationship with material fabrication techniques, reliable multiple value storage device fabrication still remains a challenge. Also, the detailed mechanism is disputed and still remains unclear. This has also impeded the development and application of multiple value storage.

In the current report, we demonstrate a multi-value storage system based on a nano-electronic–mechanical mechanism using reconnectable graphene flakes (GFs). Contact-rupture hysteresis in the graphene structure was demonstrated, and relatively stable storage windows were observed. We show both binary- and multi-value storage in this system, and the mechanisms are clearly demonstrated based on detailed *in situ* observations.

Experiments

A nanofactory TEM-STM holder was used for *in situ* manipulation and probing of the electrical properties of the system. A 200 keV TECNAI G20 transmission electron microscope (TEM, FEI

[a]*SEU-FEI Nano-Pico Center, Key Laboratory of MEMS of Ministry of Education, School of Electrical Science and Engineering, Southeast University, 210096 Nanjing, China. E-mail: wn@seu.edu.cn*

[b]*Laboratory of Condensed Matter Spectroscopy and Opto-Electronic Physics, Key Laboratory of Artificial Structures and Quantum Control (Ministry of Education), Department of Physics and Astronomy, Shanghai Jiao Tong University, Shanghai, China*

[c]*National Laboratory of Solid State Microstructures, College of Engineering and Applied Sciences, Nanjing University, 210093 Nanjing, China*

† Electronic supplementary information (ESI) available. See DOI: 10.1039/c6ra11115g

This journal is © The Royal Society of Chemistry 2016

Published on 20 July 2016. Downloaded by Southeast University - Jiulonghu Campus on 25/12/2016 13:59:32.

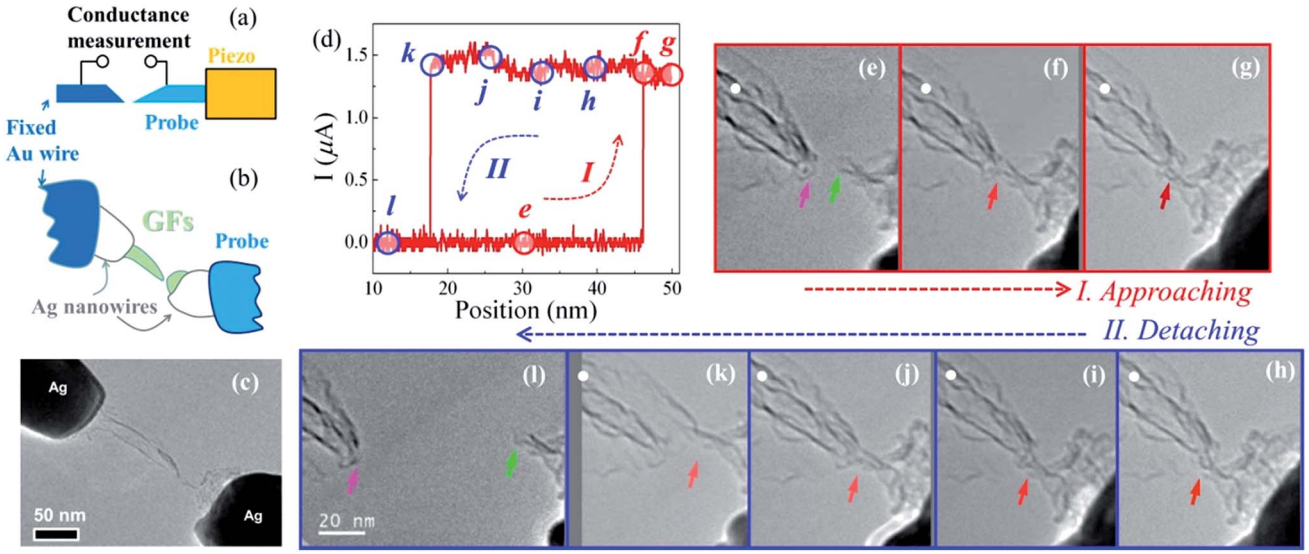

Fig. 1 (a) Schematic of the nanofactory TEM-STM measurement and manipulation mechanisms. (b) Sample structure of the current experiments; GFs = graphene flakes. The structure is in accordance with that shown in the TEM image in (c). (d) The current–position relationship shows a two-level storage mechanism during approaching ((e) to (g)) and withdrawing ((h) to (l)) of the GFs tips. TEM images (e) to (l) share the same scale bar.

Company) was used for observation and image recording. Graphene flakes (GFs) were obtained by heating amorphous carbon *in situ* to burning in the high vacuum TEM chamber (greater than 2×10^{-4} Pa). Two segments of gold wire (purity > 4 N, diameter 0.25 mm) were used as electrodes and mounted in the TEM-STM holder. One of the gold wires was fixed (and electrically grounded), and the other was allowed to move in three dimensions (see Fig. 1(a)). The gold wire tip was dipped into an ethanol dispersion of Ag nanowire,[9] removed, and allowed to dry naturally; thus, Ag nanowire was attached firmly onto the Au surface.

Graphene flakes were fabricated *in situ* inside the TEM chamber. Amorphous carbon was used as the starting phase; this may be introduced by electron beam induced material deposition or simply formed on Ag nanowires by atmospheric absorption of floating organic molecules after long-time storage. After the contacting of two Ag nanowires with a region of amorphous carbon between them, a high current pulse was applied and passed through the contact. This caused the graphization of the amorphous carbon. Numerous graphene flakes were stacked and connected between the gold electrodes (see Fig. 1(b) and (c)), in accordance with our previous observations.[10] By manipulation of the movable gold electrode, the connections of the graphene flakes could be mechanically broken or reconnected, and their electrical properties could be measured.

Results and discussion

Good metallic contact between Au wires and Ag nanowires is confirmed by connecting two Ag wires without amorphous carbon or graphene flakes between them.[9] The TEM image in Fig. 1(c) shows good contact between the GFs and the Ag nanowire. The GFs were found to be stacked randomly and formed a free-standing sheet with a typical thickness of ~3 nm, as determined from the TEM images, connected between the two Ag nanowire tips. The sheet of GFs can be fractured by applying a voltage pulse followed by the creation of two sharp tips, as indicated by colored arrows in Fig. 1(e). The GFs can be connected by bringing the probe towards the fixed side. A constant voltage of 2 V was applied to the probe as it approached the fixed side (with a velocity of 6.5 nm s^{-1}). The contact of the GFs tips can be verified directly from the TEM images as well as from the change of current. Once contact was made (indicated by the red arrow in Fig. 1(f)), a jump in the current was observed (site "f", Fig. 1(d)). A projected contact size of ~8 nm was observed. As the probe approached the GFs sheet, a slight deformation occurred on the left side (fixed side, Fig. 1(g)) due to compression deformation, while the current level remained unchanged (site "g", Fig. 1(d)). Retraction of the probe (with a velocity of 6.5 nm s^{-1}, see Fig. 1(h) to (k)) also showed little change in the current level (site "h" to "k", Fig. 1(d)) until the final contact fracture (Fig. 1(l) and site "l", Fig. 1(d)). Fig. 1(j) and (k) also showed strain (maximum strain achieved at ~12.8% for the left side GFs and ~4.7% for the right side GFs, Fig. 1(k), from the TEM images) of the GFs around the contact, as judged from the *in situ* observations. The final fracture position did not overlap with the initial contact position, as observed in both the current–position curve and the TEM image in Fig. 1(l). A hysteresis window with a size of ~26 nm was observed. Binary current level distribution was observed in Fig. s1(a),† indicating a two-level storage mechanism.

Careful checking of the TEM images revealed that both the GFs tip structures on the right side (probe side) and the left side (fixed side) changed very little after the contact was ruptured

Published on 20 July 2016. Downloaded by Southeast University - Jiulonghu Campus on 25/12/2016 13:59:32.

(cyan and green arrows in Fig. 1(e) and (l)), indicating that the contact was fractured almost at the same site where the contact occurred. Indeed, our repeated approach and retraction measurements show similar hysteresis windows. The window size exhibited a weak exponential-type decrease during the initial ten to fifty measurements before a relatively constant window size was achieved (Fig. s2(a)†). After a longer measurement sequence, the window size tended to be distributed around an average value (Fig. s2(b)†). The exponential dependence of the window size at the initial stage may be caused by accelerated structure alteration under the energetic electron irradiation. This is because a 200 keV e-beam has sufficiently high energy to change the atomic structure of carbon based materials[11]. However, the e-beam effect can be excluded as a main source for the structure change during our experiment period, because evident structure change is observable on a time scale (several minutes) much larger than our *in situ* experimental time (several seconds).

The constant current level under the contact state (Fig. 1(d)) indicated that a constant contact area was maintained under both compression (Fig. 1(g)) and pulling (Fig. 1(j) and (k)). A notably stable contact was actually realized once the graphene tip contact was formed. In another aspect, the small variation of the fractured contact tip structure indicated that the structure rupture did not occur at exactly the same place. This small but limited structure alteration of the contact tips may be due to the intrinsically small graphene flake size and the high tendency of structure defect formation at their connecting interface. The connecting interface may be the weak point and contribute to the rupturing of the contact. Therefore, the structure change of the contact tip can result from the addition or loss of one or several graphene flakes. Moreover, from Fig. 1(d), a current density on the order of $\sim 10^7$ A cm^{-2} can be calculated when considering a rectangular contact with a thickness of $\sim$2 nm and a length of $\sim$8 nm. This current density is comparable to that of carbon nanotube structures, indicating that high quality, firm contact was readily achieved once the GFs contact was established.

In situ current–voltage (*I–V*) scans (Fig. s3(a)†) showed symmetric characteristics. This excluded the possibility of electrical asymmetry induced by different GFs–metal local contact structures or contact areas. As a matter of fact, the *I–V* should be mainly contributed by the contact site region due to the relatively small contact size. Analysis of the *I–V* curves revealed that the space charge limited current (SCLC) was the dominant conducting mechanism (Fig. s3(b)†), which verified the contact-dominated current.[12]

The fundamental contact hysteresis can be interpreted based on two graphene electrodes under constant electrical bias, as shown in Fig. 2. Initially (Fig. 2(a)), two graphene flake electrodes were placed opposite to each other with a tip-to-tip distance of d_0, corresponding to an open state (position "a" in Fig. 2(g)). The tips approached each other, inducing tip contact (Fig. 2(b)) and an increase in the current level (position "b" in Fig. 2(g)). Carbon–carbon (C–C) bonds formed at the contact site help to connect the two GF electrodes and support the current flow. Further approach of the tips, however, results in no further increase in the current level (position "c" in Fig. 2(g)), as the contact remains the same size although structure deformation is observed (Fig. 2(c)). A slight withdrawal also results in the same current level because the contact is still retained (Fig. 2(d), position "d" in Fig. 2(g)). The C–C bonds connecting the two GF electrodes contribute a contact strength that prevents the contact from being ruptured when the probe position (Fig. 2(e), position "e" in Fig. 2(g)) is passing through the initial position (Fig. 2(b)), unless a relatively larger withdrawal distance is applied (Fig. 2(f), position "f" in Fig. 2(g)). This mechanism generates a hysteresis window in the current

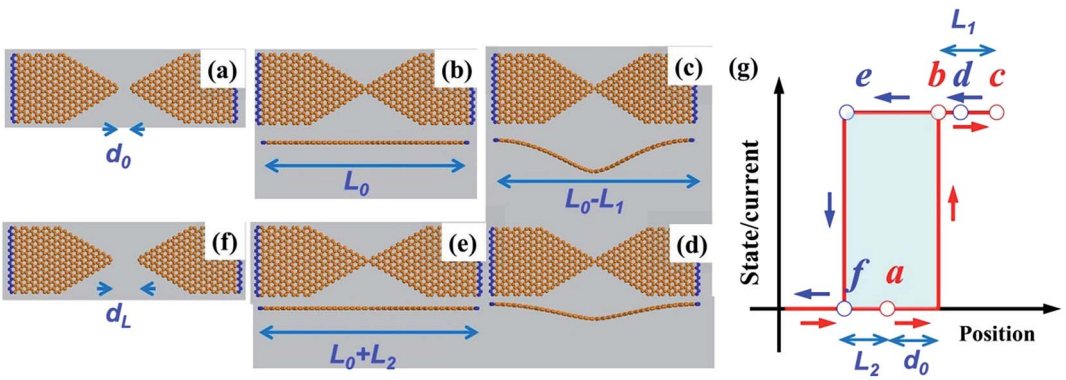

Fig. 2 Schematic of the nano-electronic–mechanical memory mechanism using GFs. (a) Two graphene flakes tip-to-tip with distance d_0 represent the initial state. (b) Tip contact resulted in an electrical connection. L_0 is the reference length when the tips are just in contact. Both the plane view and the side view are shown. (c) Further approach of the tips induced elastic deformation, while the electrical connection was retained. L_0 was reduced by L_1. (d) The electrical connection was retained as the tip was subsequently withdrawn, which reduced the elastic deformation. (e) Further tip withdrawal caused elastic deformation of the graphene flakes, while the electrical connection was retained. L_0 was extended by L_2 due to elastic deformation. (f) Tip-to-tip distance of d_L when the contact was just ruptured. $d_L > d_0$ holds due to the elastic deformation. (g) Change of the current level or state with position in accordance with the change of the contact structure. "a" to "f" corresponds to the situations shown in (a) to (f). Note that single crystal graphene sheets are shown here for clarity; these should be more appropriately interpreted as inter-connecting GFs, as seen in our experiment.

 This journal is © The Royal Society of Chemistry 2016

Published on 20 July 2016. Downloaded by Southeast University - Jiulonghu Campus on 25/12/2016 13:59:32.

(or resistivity, or state)–position relationship. The added length of the initial two GFs electrodes (with the initial distance of L_0, Fig. 2(b)) was extended to $L_0 + L_2$, with L_2 being the increased length due to elastic deformation during withdrawal, and was decreased to $L_0 - L_1$, with L_1 being the elastic deformation during approach. The window size (W) should be fulfilled by:

$$W = d_0 + L_2 \quad (1)$$

$$L_2 = S \cdot L_0 / Y \quad (2)$$

where S is the contact strength and Y is the Young's modulus of the structured GFs. It is worth noting that due to the relatively large Young's modulus of perfect graphene, L_2 is rather small; this results in a very small window size. Therefore, in order to achieve a larger window size, the structures depicted as single crystal graphene should be replaced by sheets of GFs with large amounts of three-dimensional compacted GFs structures, with Young's moduli Y that are tunable *via* density or package style.[13] GFs structures obtained by *in situ* thermal activation (as obtained in this work) or by reduced chemically derived graphene oxide with good flake size control may be used for nano-electronic–mechanical storage.

Multi-level storage was also realized by using a similar mechanism to that presented in Fig. 3(a). The current–position relationship shows a typical three-level mechanism (see also Fig. s1†). This mechanism was realized by adding another contact to the two-level system, as described in Fig. 3(b) to (j). Fig. 3(b) to (d) show, in sequence, the approach of the GFs electrode ("b" to "d" in Fig. 3(a)) for the formation of the second contact (indicated by a blue arrow in Fig. 3(e)) after the first contact (red arrows in the figures) was already formed. In Fig. 3(c), the sites used for the formation of the second contact are indicated by green and cyan arrows on the opposing GFs tips, respectively. Formation of the second contact caused the current to jump again, as indicated at "e" in Fig. 3(a). Further approach of the tip slightly pressed the GFs sheet on the left side (Fig. 3(f)) and resulted in very limited current variation ("f" in Fig. 3(f)). Subsequent withdrawal of the tip resulted in well-preserved electrical and structural connections (Fig. 3(g), "g" in Fig. 3(a)) until the final contact rupture (Fig. 3(h), "h" in Fig. 3(a)). A storage window with a size of ~18 nm was observed. The contact sites also showed little structure change after the rupture, as can be seen from a comparison between Fig. 3(c) and (i). The first contact was also well maintained, as verified by the same current level at positions "i" and "b", "c" and "d" in Fig. 3(a); this contact was finally ruptured, resulting in zero current (Fig. 3(j), "j" in Fig. 3(a)).

It can be readily seen in Fig. 3(b) to (i) that the first contact was well maintained; thus, the higher current level after the second contact formation resulted from both of the contacts being connected in parallel. The second contact thus contributed a current of ~3.5 μA, corresponding to a current density on the order of $\sim 10^7$ A cm^{-2} by considering a rectangular contact with thickness ~2 nm and length ~15 nm. This is in accordance with the above estimation. The *I–V* curves (Fig. s3(a)†) of the contacts (including the first and the second) also show similar symmetric characteristics (SCLC) with the same slope (Fig. s3(b)†), suggesting that increased current level should be the only result of the increased contact area.

The three-level mechanism can be interpreted based on the formation of two contacts with different distances, as schematically shown in Fig. 3(k). When two oppositely placed GFs approach each other, the contact "C1" forms firstly because of the smaller distance, which contributes to a current jump. Further approach causes a shape deformation of "C1", with a slight current change. When the "C2" contact is formed, the second current jump appears and remains constant as the GFs approach further. Separation of the two GFs induces the rupture of the contacts in reverse order and accordingly gives the stepped current–position relationship. Considering the window

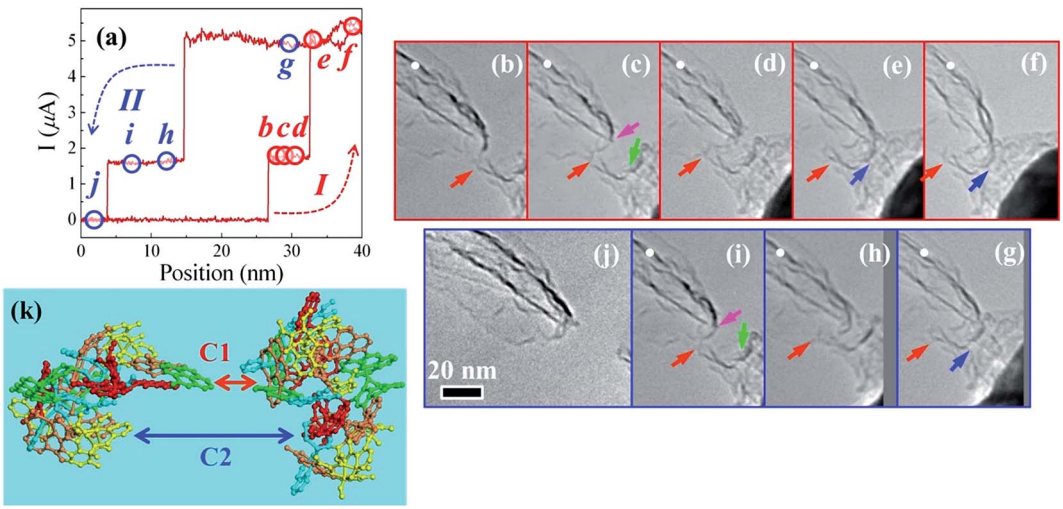

Fig. 3 (a) The current–position relationship shows a three-level mechanism. TEM images presented in (b) to (j) show the approach and formation ((b) to (f)) as well as the withdrawal and rupture ((g) to (j)) of the contact(s). The TEM images share the same scale bar. (k) GFs with two contact pairs, indicated by C1 and C2, with different distances. Colored atoms indicate individual GFs.

Published on 20 July 2016. Downloaded by Southeast University - Jiulonghu Campus on 25/12/2016 13:59:32.

sizes of the two contacts, W_1 and W_2, respectively, the initial distance between the first contact, d_0, and the distance between "C1" and "C2", L, the three-level mechanism requires:

$$W_2 > d_0 + L \quad (3)$$

$$W_1 > d_0 \quad (4)$$

Eqn (3) and (4) imply that in order to realize the three-level mechanism, the two hysteresis windows should have some regional overlap in order to obtain the stored state. Although more windowed current–position relationships were observed in some of our experiments (for example, as shown in Fig. s4(a) and (b)†), up to four current level steps were observed, they failed to realize the window overlap; thus, they were not usable for storage. Levels greater than three are theoretically possible based on the current mechanism; however, they are actually more difficult to achieve and may require further consideration of their material, mechanical and structure design.

The contact hysteresis of the GFs plays the key role in nano-electronic–mechanical storage mechanisms. It was found that the contact hysteresis was less observable under low current density (as shown in Fig. s5†), where very small hysteresis windows (on the order of ~0.5 nm) were observed, indicating low contact strength. Consequently, high current density was suggested to induce better contact strength through an *in situ* spot-welding mechanism that takes place during contact of the GFs. The occurrence of a thermal effect at the contact may promote inter-edge connection of the graphene flakes in order to achieve physical carbon bond connections rather than weak van der Waals interactions.

Summary

We demonstrated a nano-electronic–mechanical mechanism using graphene flakes that could be used for multiple value storage. The detailed mechanisms were studied by *in situ* transmission electron microscope observations, accompanied by nano-manipulation and probing of the electrical properties of the system. Repeatable two- and three- level state storage processes were shown by contacting two GFs electrodes with contact hysteresis. A spot-welding mechanism during the contact hysteresis was suggested. The relationships of some key parameters to the storage mechanism, including the window size, the elastic deformation of the GFs and the Young's modulus of the materials, were also discussed.

Acknowledgements

This study is supported by the National Basic Research Program of China (Grant No. 2015CB352106), the National Natural Science Foundation of China (Grant No. 61370042, 61504030, 61006011, 11304197 and 11374136), and Specialized Research Fund for the Doctoral Program of Higher Education (Grant No. 20100092110014).

References

1 R. E. Simpson, P. Fons, A. V. Kolobov, T. Fukaya, M. Krbal, T. Yagi, *et al.*, Interfacial phase-change memory, *Nat. Nanotechnol.*, 2011, **6**, 501–505.
2 D. Loke, J. M. Skelton, W.-J. Wang, T.-H. Lee, R. Zhao, T.-C. Chong, *et al.*, Ultrafast phase-change logic device driven by melting processes, *Proc. Natl. Acad. Sci. U. S. A.*, 2014, **111**, 13272–13277.
3 S. Jandhyala, G. Mordi, D. Mao, M.-W. Ha, M. A. Quevedo-Lopez, B. E. Gnade, *et al.*, Graphene–ferroelectric hybrid devices for multi-valued memory system, *Appl. Phys. Lett.*, 2013, **103**, 022903–022905.
4 Y. P. Yao, Y. K. Liu, S. N. Dong, Y. W. Yin, S. W. Yang and X. G. Li, Multi-state resistive switching memory with secure information storage in $Au/BiFe_{0.95}Mn_{0.05}O_3/La_{5/8}Ca_{3/8}MnO_3$ heterostructure, *Appl. Phys. Lett.*, 2012, **100**, 193504–193506.
5 B. Kundys, V. Iurchuk, C. Meny, H. Majjad and B. Doudin, Sub-coercive and multi-level ferroelastic remnant states with resistive readout, *Appl. Phys. Lett.*, 2014, **104**, 232905–232907.
6 G. Yang, H.-Y. Chen, L. Ma, Y. Shao and Y. Yang, Study of multi-ON states in nonvolatile memory based on metal–insulator–metal structure, *Appl. Phys. Lett.*, 2009, **95**, 203506–203508.
7 V. Iurchuk, H. Majjad, F. Chevrier, D. Kundys, B. Leconte, B. Doudin, *et al.*, Multi-state and non-volatile control of graphene conductivity with surface electric fields, *Appl. Phys. Lett.*, 2015, **107**, 182901–182903.
8 K. M. M. Habib, F. Zahid and R. K. Lake, Multi-state current switching by voltage controlled coupling of crossed graphene nanoribbons, *J. Appl. Phys.*, 2013, **114**, 153710–153717.
9 S. Tang, S. Vongehr, N. Wan and X. Meng, Rapid synthesis of pentagonal silver nanowires with diameter-dependent tensile yield strength, *Mater. Chem. Phys.*, 2013, **142**, 17–26.
10 N. Wan, L.-T. Sun, S.-N. Ding, T. Xu, X.-H. Hu, J. Sun, *et al.*, Synthesis of graphene–CNT hybrids *via* joule heating: structural characterization and electrical transport, *Carbon*, 2013, **53**, 260–268.
11 J. A. Rodríguez-Manzo, F. Banhart, M. Terrones, H. Terrones, N. Grobert, P. M. Ajayan, *et al.*, Heterojunctions between metals and carbon nanotubes as ultimate nanocontacts, *Proc. Natl. Acad. Sci. U. S. A.*, 2009, **106**, 4591–4595.
12 A. A. Talin, F. Léonard, B. S. Swartzentruber, X. Wang and S. D. Hersee, Unusually strong space-charge-limited current in thin wires, *Phys. Rev. Lett.*, 2008, **101**, 076802–076806.
13 Y. Wu, N. Yi, L. Huang, T. Zhang, S. Fang, H. Chang, *et al.*, Three-dimensionally bonded spongy graphene material with super compressive elasticity and near-zero Poisson's ratio, *Nat. Commun.*, 2015, **6**, 6141–6149.

 This journal is © The Royal Society of Chemistry 2016